Single Mode Lindblad Description of the Parametric Instability

bachelor's thesis

Submitted to the Faculty of Mathematics, Computer Science and Natural Sciences at RWTH Aachen University

presented by

Steven Kim

under the supervision of

Prof. Dr. Fabian Hassler

JARA-Institute for Quantum Information

07/2021

Abstract

In contrast to a coherent drive, a parametric drive can lead to an exponential increase of the oscillation amplitude. This thesis analyzes the instability threshold of parametrically driven oscillators, using the Lindblad Master equation for open quantum systems. Above the threshold the harmonic oscillator is unstable, but anharmonicities, such as they are present for a Duffing oscillator, stabilize the system. Analytical expressions for the steady states of the expectation values of the occupation number operator above and below the threshold are derived. We show how to extract the modes of the Lindbladian and demonstrate how it can be approximated by a single mode close to the threshold.

Contents

Chapter 1

Introduction

Due to friction, an oscillator loses momentum during its oscillation and comes to a halt. A coherent drive can be employed to sustain the oscillation as it is in the case of a child on a swing being pushed by its parents. But there is a second way to maintain the oscillation. The child can vary the moment of inertia of the swing by periodically standing up and sitting down. The motion has to be done twice as fast as the swings oscillation and results in self-sustained oscillations for sufficiently strong driving strengths. This is called a parametric drive.

The most common use of parametrically driven oscillators is the amplification of signals, with much lower signal-noise ratio than a transistor based amplifier [1]. This can be done by a varicap diode which uses a voltage-dependent capacitance [2]. It can also be used as a frequency mixer or as a voltage controlled oscillator.

In Ch. 2 of this thesis, the classical parametric harmonic oscillator is investigated. We describe how a rotating-frame approximation is done and calculate the instability threshold where the system reaches self-sustained oscillation. Then, we consider the Duffing oscillator and show that it stabilizes the dynamics above the threshold due to its non-linearity. Chapter 3 gives a short introduction to open quantum systems and discusses how dissipative dynamics can be described. As an example, we take a look at the dissipative harmonic oscillator. Chapter 4 deals with the quantum parametric oscillator and how the expectation values of the ladder operators and occupation number operator behave in time. We obtain that the classical threshold matches with the quantum mechanical instability threshold. In addition, we show that the classical threshold transition of the Duffing oscillator is washed out by quantum effects and that the Duffing oscillator reaches steady coherent states that match with the classical calculations. In the last Ch. 5, we diagonalize the Hamiltonian of the parametric oscillator in two ways. One of them is the symplectic diag-

onalization which is also of use for the Lindbladian of the open system. For the parametric harmonic oscillator, the system can be described by two Lindblad modes where only one is affected by the instability threshold. Therefore, the Lindbladian can be approximated close to the threshold resulting in faster computation times.

Chapter 2

Classical parametric oscillator

2.1 RWA and classical threshold

The equation of motion for the parametrically driven damped harmonic oscillator is given by

$$\ddot{q} + \gamma\dot{q} + \omega_0^2 q + 2\omega_0\varepsilon\sin(2\omega t)q = 0. \tag{2.1}$$

The first three terms of this equation describe the damped harmonic oscillator, while the last term describes the parametric drive with amplitude ε and driving frequency $2\omega = 2\omega_0 + \Delta$. Here, Δ is the detuning and equals zero for resonant driving. To solve this equation, we make the ansatz

$$q(t) = x(t)\sin(\omega t) + y(t)\cos(\omega t) \tag{2.2}$$

where $x(t)$ and $y(t)$ are functions that vary slowly with time. For the parametric drive we use

$$\sin(2\omega t)\cos(\omega t) = \frac{1}{2}\left[\sin(\omega t) + \sin(3\omega t)\right] \tag{2.3}$$

$$\sin(2\omega t)\sin(\omega t) = \frac{1}{2}\left[\cos(\omega t) - \cos(3\omega t)\right]. \tag{2.4}$$

The application of the addition theorems in Eq. (2.3) and (2.4) produces driving terms that oscillate with frequency ω and off-resonant fast oscillating terms with frequency 3ω. We are interested in a weakly damped and small detuned system ($\Delta, \gamma \ll \omega_0$) and therefore set the according terms equal to zero. Furthermore, the fast oscillating terms are neglected. This is called the rotating-frame approximation and leads to

$$\cos(\omega t)\left(\dot{y} + \frac{\Delta}{2}x - \frac{\varepsilon - \gamma}{2}y\right) + \sin(\omega t)\left(\dot{x} + \frac{\Delta}{2}y + \frac{\varepsilon + \gamma}{2}x\right) = 0. \tag{2.5}$$

Since the cosine and sine cannot cancel each other out, the respective coefficients equal zero. The resulting differential equations can be described with a Hamiltonian via

$$\dot{x} = -\frac{\gamma}{2}x + \frac{\partial H}{\partial y} \tag{2.6}$$

$$\dot{y} = -\frac{\gamma}{2}y - \frac{\partial H}{\partial x} \tag{2.7}$$

where the Hamiltonian H is given by $H = -\frac{\varepsilon}{2}xy + \frac{\Delta}{4}(x^2 + y^2)$. For $\gamma = 0$ we obtain the classical Hamilton equations. Note that y is not the impulse but the second quadrature. We move into the complex plane by defining a complex number $\alpha = \frac{1}{\sqrt{2}}(x + iy)$. The Hamiltonian and the equation of motion result in

$$H(\alpha, \bar{\alpha}) = \frac{\Delta}{2}|\alpha|^2 + \frac{i\varepsilon}{4}(\alpha^2 - \bar{\alpha}^2) \tag{2.8}$$

$$\dot{\alpha} = -\frac{\gamma}{2}\alpha - i\frac{\partial}{\partial\bar{\alpha}}H(\alpha, \bar{\alpha}), \tag{2.9}$$

where the time evolution of $\bar{\alpha}$ is the complex conjugate of Eq. (2.9). The coupled differential equation is then given by

$$\frac{d}{dt}\begin{pmatrix} \alpha \\ \bar{\alpha} \end{pmatrix} = -\frac{1}{2}\begin{pmatrix} i\Delta + \gamma & \varepsilon \\ \varepsilon & -i\Delta + \gamma \end{pmatrix}\begin{pmatrix} \alpha \\ \bar{\alpha} \end{pmatrix}. \tag{2.10}$$

The eigenvalues of the matrix are $\lambda_\pm = \frac{1}{2}(\pm(\varepsilon^2 - \Delta^2)^{1/2} - \gamma)$. The solution is an exponential decay which reaches a steady state at zero, as long as both eigenvalues have a negative real part. This means that the system reaches a steady state for times much larger than λ_+^{-1}, if the moduled drive $(\varepsilon^2 - \Delta^2)^{1/2}$ is smaller than the damping γ. When the moduled drive is bigger than the damping, the system transfers into self-sustained oscillations and does not reach a steady state anymore. For resonant driving, this instability threshold lies at $|\varepsilon| = \gamma$. If there is detuning, the threshold shifts to $|\varepsilon| = (\gamma^2 + \Delta^2)^{1/2}$. Another effect of the detuning is that the solution for α gets an imaginary part that only vanishes for resonant driving, $\Delta = 0$, if there is no imaginary part to start with. This can be seen in Fig. 2.1 and Fig. 2.2.

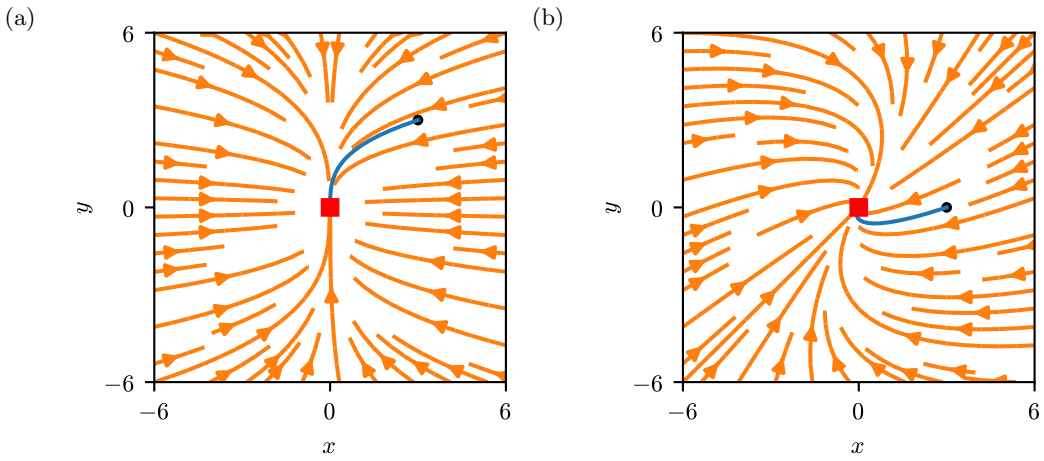

Figure 2.1: Streamplot below the threshold. (a) $\Delta = 0$. All streamlines, indicated by the orange lines, point to the origin (red square). The blue line represents an example for a trajectory with the initial value (black dot) with $\alpha_i = 3(1+i)$. (b) $\Delta = 0.5\gamma$. All streamlines point to the origin again. Although the initial value is completely real ($\alpha_i = 3$) the trajectory still shifts into the complex plane.

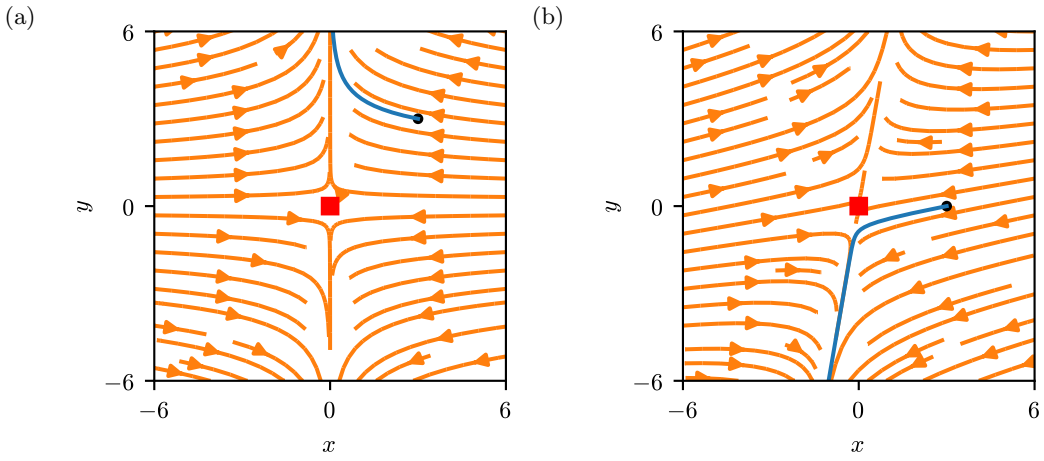

Figure 2.2: Streamplot above the threshold for $\varepsilon = 1.5\gamma$. (a) $\Delta = 0$. All streamlines (orange lines) point away from the origin. The blue line represents an example for a trajectory with the initial value $\alpha_i = 3(1+i)$. While the real part still decays to zero, the imaginary part diverges. (b) $\Delta = 0.5\gamma$ with the initial value $\alpha_i = 3$. The whole solution for α diverges.

2.2 Duffing oscillator

In reality, an oscillator does not start to oscillate with a divergent amplitude above a certain threshold. The system gets stabilized, which is described by an anharmonicity. As for the the Duffing oscillator, the Hamiltonian gets extended by a new term which is described by $u|\alpha|^4$, with a small parameter u. With the new Hamiltonian and Eq. (2.9) we find

$$\dot{\alpha} = -\frac{1}{2}(i\Delta + \gamma)\alpha - (\frac{\varepsilon}{2} + 2iu\alpha^2)\bar{\alpha}. \tag{2.11}$$

For $\Delta = 0$ the equation is still imaginary, even if the initial value of α is real. This means that the system is not driven at the resonance frequency anymore and is detuned due to the non-linearity.

This coupled differential equation cannot be solved anymore. Nevertheless, it is possible to determine the steady states, by setting $\dot{\alpha}$ equal to zero and solving for α. For the following, we assume $\Delta = 0$. We obtain three steady state solutions

$$\alpha_0 = 0 \quad \text{and} \quad \alpha_{1,2} = \pm\sqrt{\frac{i(\varepsilon^2 - \gamma^2) - \gamma\sqrt{\varepsilon^2 - \gamma^2}}{4\varepsilon u}}. \tag{2.12}$$

To perform a stability analysis of the steady states, we do a linear expansion. The solutions are stable when all eigenvalues have a negative real part because the fluctuation $\delta\alpha$ decays to zero. By expanding Eq. (2.11) we get

$$\frac{d}{dt}\begin{pmatrix} \delta\alpha \\ \delta\bar{\alpha} \end{pmatrix} = -\frac{1}{2}\begin{pmatrix} \gamma + 8iu|\alpha|^2 & \varepsilon + 4iu\alpha^2 \\ \varepsilon - 4iu\bar{\alpha}^2 & \gamma - 8iu|\alpha|^2 \end{pmatrix}\begin{pmatrix} \delta\alpha \\ \delta\bar{\alpha} \end{pmatrix}. \tag{2.13}$$

The eigenvalues are $\lambda_{1,2} = -\frac{\gamma}{2} \pm \frac{1}{2}(\varepsilon^2 - 8\varepsilon u\,\mathrm{Im}(\alpha^2) - 48u^2|\alpha|^4)^{-1/2}$. Below the threshold, there is only α_0 as the steady stable state. Above the threshold, α_0 becomes unstable and $\alpha_{1,2}$ are the stable steady states. This means that the threshold can be imagined as a transition from a paraboloid to a double-well potential, which is shown in Fig 2.3. By rewriting Eq. (2.11) back in its real and imaginary part we obtain a vector field $\vec{F}(x, y)$

$$\dot{x} = \mathrm{Re}(\dot{\alpha}) = \frac{1}{\sqrt{2}}(\dot{\alpha} + \dot{\bar{\alpha}}) = 2uy(x^2 + y^2) - x\frac{\varepsilon + \gamma}{2} = F_x \tag{2.14}$$

$$\dot{y} = \mathrm{Im}(\dot{\alpha}) = \frac{1}{\sqrt{2}i}(\dot{\alpha} - \dot{\bar{\alpha}}) = -2ux(x^2 + y^2) + y\frac{\varepsilon - \gamma}{2} = F_y. \tag{2.15}$$

These are solved by the forward-Euler method described in Appendix B.

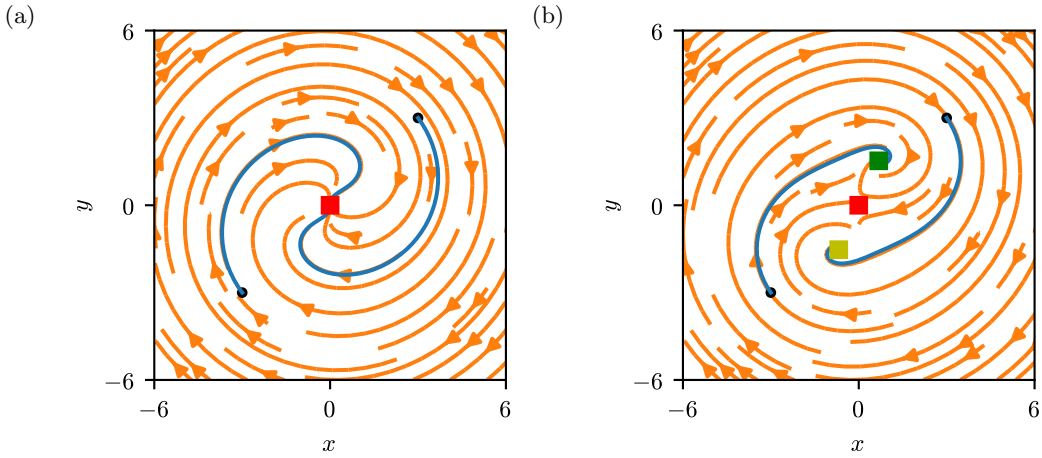

Figure 2.3: Streamplot of the duffing oscillator with $u = 0.1\gamma$ and for the initial values $\alpha_i = \pm 3(1 + i)$. (a) Streamplot below the threshold for $\varepsilon = 0.5\gamma$. All streamlines point to the origin and the solution reaches the steady state at $\alpha_0 = 0$ independently of the initial value. (b) Streamplot above the threshold for $\varepsilon = 1.5\gamma$. The streamlines do not point to the origin anymore, but to the steady state solutions α_1 (green square) and α_2 (yellow square), see Eq. (2.12).

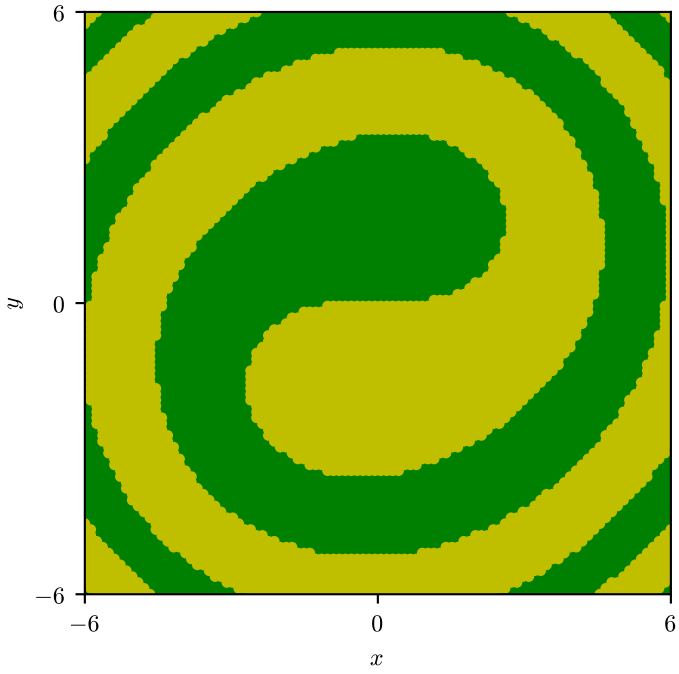

Figure 2.4: Steady state solution dependent on the initial value. For every green point the system reaches a steady state at α_1 for this initial value. The solution is α_2 for every yellow point.

Chapter 3

Open quantum systems

3.1 Lindblad Master equation

A quantum system is completely described by its density matrix

$$\rho = \sum_k p_k \left|\psi_k\right\rangle\!\left\langle\psi_k\right| . \tag{3.1}$$

It characterizes the ensemble of possible states $|\psi_k\rangle$ with probability $p_k \geq 0$ and can represent both, pure and mixed states. For a pure state the density matrix reduces to $\rho = |\psi\rangle\langle\psi|$ and the description by the wavefunction can be used instead. But these pure states are idealized descriptions and do not represent possible mixtures that occur in experiments or nature, as for the case of an open system with dissipative dynamics. This is the reason why it is useful to characterize the system by its density matrix. When time elapses, the ensemble can change its properties and the density matrix evolves. The time evolution of the closed system is described by the von-Neumann equation

$$\frac{\partial \rho}{\partial t} = -i[H, \rho], \tag{3.2}$$

with the Hamiltonian H and $\hbar = 1$. As already mentioned, open systems interact with their environment which leads to absorption and emission of photons with frequency ω_0. The dissipative dynamics are described by the Lindblad Master equation [3]

$$\frac{\partial \rho}{\partial t} = \mathcal{L}\rho = -i[H, \rho] + \gamma\,(1 + n_0)\,J[a](\rho) + \gamma n_0 J[a^\dagger](\rho) \tag{3.3}$$

where γ is the decay rate, $n_0 = (e^{\beta\omega_0} - 1)^{-1}$ the Bose–Einstein distribution of the thermal photonic bath with $\beta = 1/(k_B T)$ and $J[a](\rho)$ a superoperator

defined by

$$J[a](\rho) = a\rho a^\dagger - \frac{1}{2}\{a^\dagger a, \rho\}. \tag{3.4}$$

The Lindblad Master Eq. (3.3) extends the von-Neumann Eq. (3.2) with additional terms describing the dissipation. Here, the first additional term corresponds to the spontaneous and induced emission of a single photon. The second term describes the absorption of a single photon. The reason for single photon loss is dipole radiation. The dipole moment d is proportional to the position operator x which consists of the ladder operators a and $a^\dagger$. These annihilate or create a single excitation in the oscillator.

The density matrix allows us to determine the expectation value of any observable O by computing $\mathrm{Tr}(O\rho)$. For a general, time-independent observable O, the time evolution of the expectation value is calculated by

$$\frac{d}{dt}\langle O\rangle = \mathrm{Tr}(O\dot{\rho}) = i\langle[H, O]\rangle + \gamma\left(\langle a^\dagger[O, a]\rangle + \frac{1}{2}\langle[a^\dagger a, O]\rangle\right), \tag{3.5}$$

using the cyclic property of the trace, when the system is coupled to a zero temperature environment ($n_0 = 0$).

3.2 Example: Harmonic oscillator

At the beginning we take a look at the harmonic oscillator. Without an external drive there is no detuning. This means that the Hamiltonian in the rotating frame is given by $H = 0$. We can determine differential equations for the expectation values of the ladder operators and the occupation number operator $a^\dagger a$. We find $\frac{d}{dt}\langle a\rangle = -\frac{\gamma}{2}\langle a\rangle$ and $\frac{d}{dt}\langle a^\dagger a\rangle = -\gamma(\langle a^\dagger a\rangle - n_0)$, by using Eq. (3.5). The first equation is solved by an exponential decay, $\langle a\rangle(t) = e^{-\gamma t/2}\langle a\rangle(0)$. This indicates that the system reaches a steady state on the timescale γ^{-1}. The second equation can be seen as a photon current. For $\langle a^\dagger a\rangle > n_0$ the current is negative and the oscillator emits photons at the rate γ. For the other case, the oscillator absorbs photons from the environment. For $\langle a^\dagger a\rangle = n_0$ the current is zero which means that this is the steady state. The explicit solution is

$$\langle a^\dagger a\rangle(t) = n_0 + \left[\langle a^\dagger a\rangle(0) - n_0\right] e^{-\gamma t}. \tag{3.6}$$

To determine the steady state solution for the density matrix we need to set $\dot{\rho}$ in Eq. (3.3) to zero. This leads to the recursive solution $(1 + n_0)\rho_{n+1} = n_0\rho_n$ where ρ_n is the n-th diagonal element of the density matrix. This is only valid when we start on the main diagonal, e.g. in the vacuum state, because no

operation in Eq. (3.3) leads to off-diagonal values. The recursion is solved by

$$\rho_n = \frac{1}{1+n_0}\left(1-\frac{1}{1+n_0}\right)^n \tag{3.7}$$

where we demand that $\mathrm{Tr}(\rho) = 1$. This resulting probability distribution is seen in Fig. 3.1(a). The ground state has the highest probability and the probability for higher states is exponentially smaller.

It is even possible to determine the time evolution of the entries. Regarding the steady state solution, the ansatz is chosen as $\rho_n(t) = y(t)\,[1-y(t)]^n$. With the Lindblad Master equation, this leads to a differential equation for $y(t)$, $\frac{d}{dt}y = \gamma y[1-y(n_0+1)]$. The solution for ρ_n results in

$$\rho_n(t) = \frac{1}{1+n_0(1-e^{-\gamma t})}\left(1-\frac{1}{1+n_0(1-e^{-\gamma t})}\right)^n \tag{3.8}$$

where we start in the vacuum state, $\rho_0(0) = 1$.

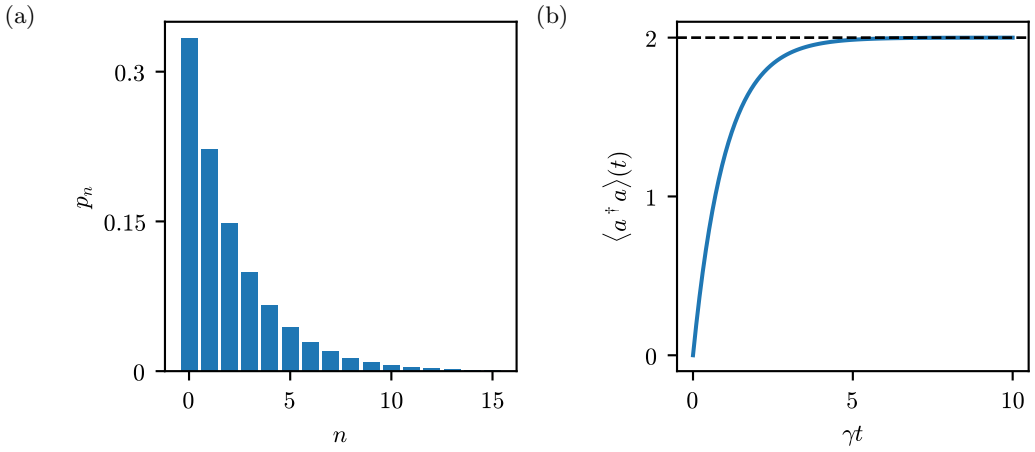

Figure 3.1: (a) Probability distribution of the steady state depending on the n-th Fock-state (Eq. (3.7) for $n_0 = 2$). The probability falls exponentially for higher states and is independent of the initial condition. (b) Time evolution of $\langle a^\dagger a\rangle$(blue line) starting in the vacuum state for $n_0 = 2$. The dotted line represents the steady state solution and is reached exponentially.

Chapter 4

Quantum parametric oscillator

4.1 Dynamics of the open system

Similar to the classical oscillator, the rotating-frame approximation can be done in quantum physics by a unitary transformation. This results in the Hamiltonian for the parametrically driven oscillator which is given by

$$H = \frac{\Delta}{2} a^\dagger a + \frac{i\varepsilon}{4}(a^2 - a^{\dagger 2}) \tag{4.1}$$

where Δ is the detuning and ε the driving amplitude. It corresponds to the classical Hamiltonian (Eq. (2.8)), by replacing the ladder operators by the complex number α. We see that the parametric drive can be obtained by a two-photon-pump.

Here, we consider the open dissipative system. Therefore the system is described by the Lindblad Master Eq. (3.3). We use Eq. (3.5) to get information about the dynamics of the expectation values and therefore about the system. We start with the linear order of the ladder operators and get

$$\frac{d}{dt}\begin{pmatrix} \langle a \rangle \\ \langle a^\dagger \rangle \end{pmatrix} = -\frac{1}{2}\begin{pmatrix} i\Delta + \gamma & \varepsilon \\ \varepsilon & -i\Delta + \gamma \end{pmatrix}\begin{pmatrix} \langle a \rangle \\ \langle a^\dagger \rangle \end{pmatrix}. \tag{4.2}$$

Replacing the expectation values of the ladder operators with α and $\bar{\alpha}$ leads to the same differential equation as with the classical oscillator, Eq. (2.10). Therefore, the classical dynamics match with the dynamics of the expectation values of quantum physical operators. There is an instability threshold at $(\gamma^2 + \Delta^2)^{1/2}$ where the system transfers into self-sustained oscillations and the system reaches a steady state for times much larger than $\lambda_+^{-1} = [(\varepsilon^2 - \Delta^2)^{1/2} - \gamma]^{-1}$.

For the quadratic order, we obtain

$$\frac{d}{dt}\begin{pmatrix}\langle a^\dagger a\rangle\\ \langle a^2\rangle\\ \langle a^{\dagger 2}\rangle\end{pmatrix} = -\begin{pmatrix}\gamma & \varepsilon/2 & \varepsilon/2\\ \varepsilon & i\Delta+\gamma & 0\\ \varepsilon & 0 & -i\Delta+\gamma\end{pmatrix}\begin{pmatrix}\langle a^\dagger a\rangle\\ \langle a^2\rangle\\ \langle a^{\dagger 2}\rangle\end{pmatrix} - \frac{1}{2}\begin{pmatrix}0\\ \varepsilon\\ \varepsilon\end{pmatrix}. \quad (4.3)$$

The eigenvalues are $\lambda_1 = -\gamma$ and $\lambda_\pm = \pm(\varepsilon^2 - \Delta^2)^{1/2} - \gamma$. As for the linear order, the moduled drive needs to be smaller than the damping to reach a steady state. If there is detuning, the threshold shifts to larger driving amplitudes and the expectation value of $\langle a^2\rangle$ gets an imaginary part, even when we start in the vacuum state. This means that taking a look onto the imaginary part tells us if there is detuning or not. While the classical solution would be zero below and infinity above the threshold, the quantum mechanical solution shows non-zero steady states below the threshold already which can be seen in Fig. 4.1(a). This means the quantum mechanical system has excitations while from the classical point of view this would not be possible. The steady state solution of the expectation value for the occupation number operator is given by

$$\langle a^\dagger a\rangle = \frac{\varepsilon^2}{4\sqrt{\varepsilon^2-\Delta^2}}\left(\frac{1}{\gamma-\sqrt{\varepsilon^2-\Delta^2}} - \frac{1}{\gamma+\sqrt{\varepsilon^2-\Delta^2}}\right) \quad (4.4)$$

Figure 4.1(b) displays that the time evolution of $\langle a^2\rangle$ gets an imaginary part only for non-resonant driving when starting in the the vacuum state.

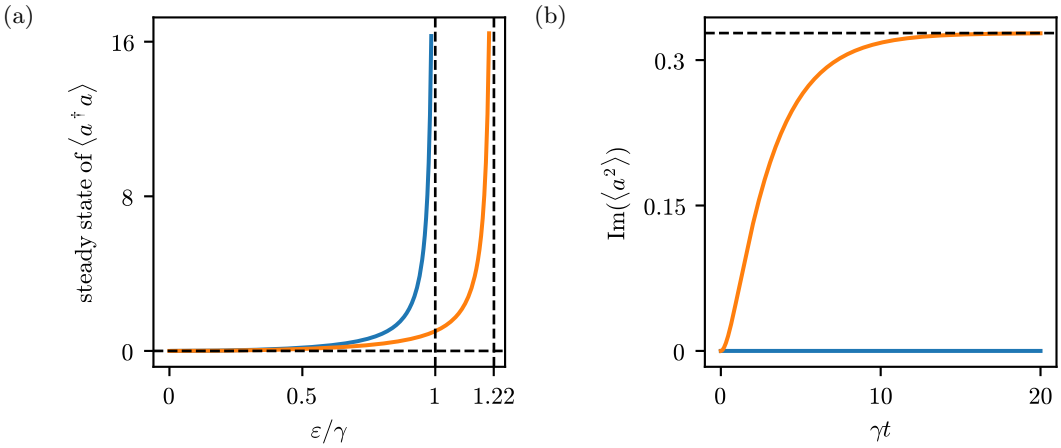

Figure 4.1: (a) Steady state solution of $\langle a^\dagger a\rangle$ for $\Delta = 0$ (blue) and $\Delta = 0.7\gamma$ (orange). For resonant driving, the steady state values of $\langle a^\dagger a\rangle$ diverge at the threshold $|\varepsilon| = \gamma$. With non-zero detuning the threshold shifts to bigger pumping strengths. (b) Time evolution of $\mathrm{Im}(\langle a^2\rangle)$ for $|\varepsilon| = 0.8\gamma$ and the same detuning. The system reaches a steady state on a timescale of λ_+^{-1} and the imaginary part only vanishes for resonant driving.

4.2 Quantum Duffing oscillator

To stabilize the system above the threshold, the Hamiltonian of the parametrically driven harmonic oscillator can be extended to the Duffing oscillator the same way as for the classical case. The Hamiltonian is given by

$$H = \frac{\Delta}{2}a^\dagger a + \frac{i\varepsilon}{4}(a^2 - a^{\dagger 2}) + ua^\dagger a^\dagger aa. \tag{4.5}$$

Here, it is not possible to find a closed system of differential equations for the expectation values anymore. The determination of them using Eq. (3.5) leads to higher orders of the ladder operators. However, it is still possible to evaluate the system numerically. In the following discussion, we focus on $\Delta = 0$. The steady state solutions in Fig 4.2 are obtained by using the eigenvalue method described in Appendix A. Far below the classical threshold at $\varepsilon = \gamma$, the solution for the quantum Duffing oscillator equals with the solution of the quantum parametric harmonic oscillator. Above the threshold, the values match with the classical solution given by $|\alpha|^2 = (\varepsilon^2 - \gamma^2)^{1/2}/(4u)$, see Eq. (2.12). While the classical solution makes a rapid change at the threshold, the quantum mechanical threshold is washed out by quantum effects (e.g. quantum fluctuations).

Figure 4.3 displays probability distributions depending on the Fock-state and the position x. We see that the maximum of the distribution lies at the steady state solutions of the classical Duffing oscillator, calculated by $x = \frac{1}{\sqrt{2}}(\alpha + \bar{\alpha})$. The probability distribution given in the Fock basis matches with the probability distribution of coherent states $|\alpha\rangle$. The dynamics of these states show very similar dynamics to the classical oscillator [4]. They can be defined as eigenstates of the annihilation operator a, $a|\alpha\rangle = \alpha|\alpha\rangle$. By demanding that they are normalized und using the representation in the Fock basis, they are given by

$$|\alpha\rangle = e^{-\frac{1}{2}|\alpha|^2} \sum_n \frac{\alpha^n}{\sqrt{n!}} |n\rangle . \tag{4.6}$$

The probability distribution corresponds to a poisson distribution by

$$\mathrm{P}(n) = |\langle n|\alpha\rangle|^2 = e^{-|\alpha|^2} \frac{|\alpha|^{2n}}{n!}. \tag{4.7}$$

This distribution matches well for driving far above the threshold because the system reaches coherent states there. This is not the case for driving below the threshold. Here, the system does not reach coherent states and therefore $\mathrm{P}(0) \neq 1$ which would follow from the classical calculations.

In Fig. 4.3(c), it is clear to see that the imaginary part of $\langle a^2 \rangle$ does not

vanish. Therefore, the system shows detuning just like the classical Duffing oscillator, see Eq. (2.11).

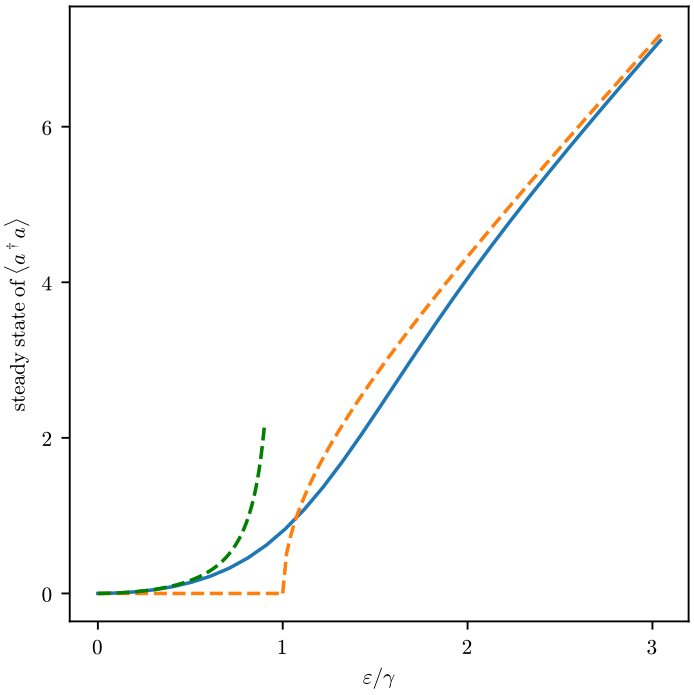

Figure 4.2: Numerical results for the steady state solution of $\langle a^\dagger a \rangle$ depending on the driving strength (blue line). The green dotted line represents the solution for the parametric oscillator at $u = 0$. The orange dotted line is the classical solution of the steady state given by $|\alpha|^2$. The found values match the expressions below and above the threshold, to the quantum parametric oscillator and the classical duffing oscillator respectively. At the classical threshold, it is not the case. This means that the classical expression only matches for strong driving. We see that the threshold is washed out by quantum effects (e.g. quantum fluctuations).

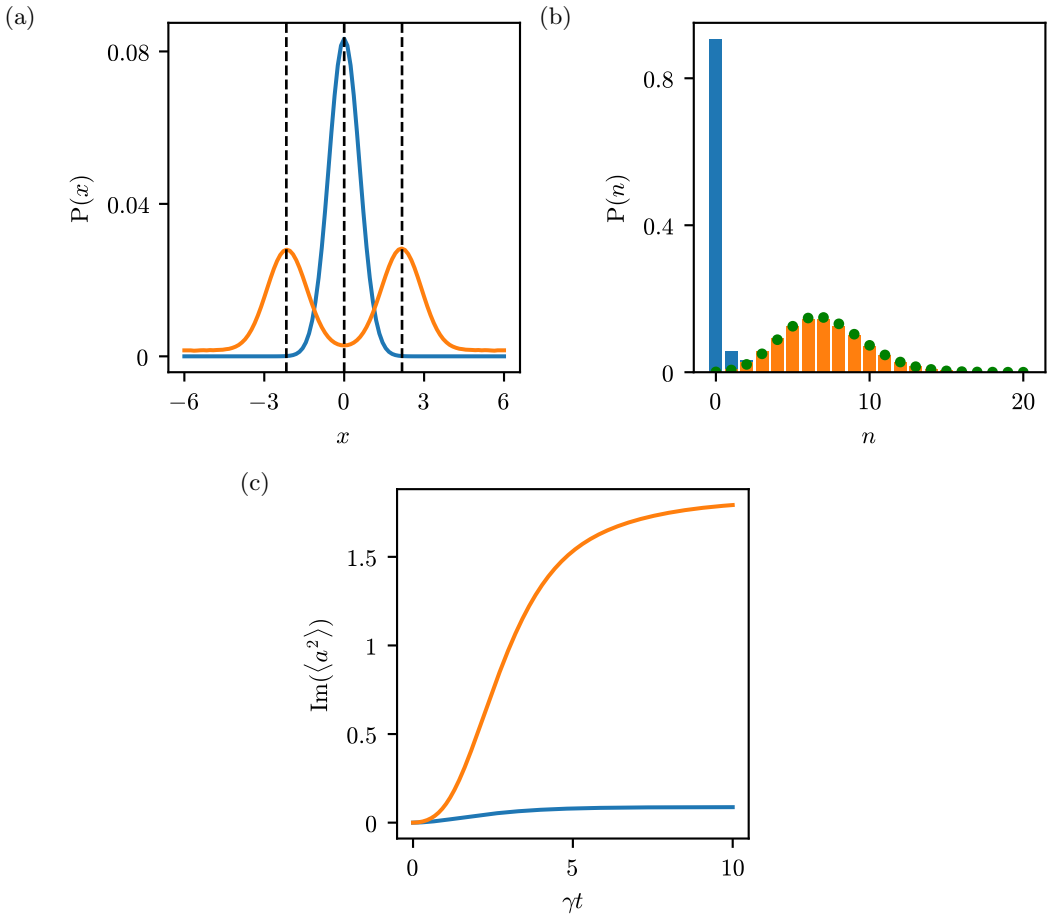

Figure 4.3: (a) Probability distribution in the steady state below the threshold (blue, $\varepsilon = 0.5\gamma$) and above the threshold (orange, $\varepsilon = 3\gamma$). The black dotted lines represent the steady state solutions for the classical Duffing oscillator. These are calculated by $x = \frac{1}{\sqrt{2}}(\alpha + \bar{\alpha})$. The maxima of the two distributions match with the classical solution and show a certain variance, as expected for a quantum mechanical system. (b) Probability distribution in the steady state below the threshold and above the threshold, depending on the n-th Fock-state. The green dots show the coherent state probability distribution above the threshold, see Eq. (4.7). Below the threshold, the ground state has the highest probability but the distribution does not match with the classical expectation. Above the threshold, the distribution widens and follows the poisson distribution of coherent states. (c) Time evolution of $\mathrm{Im}(\langle a^2 \rangle)$, below and above the threshold for $\Delta = 0$. The system is stabilized in both cases which we expect from the classical point of view. Even for $\Delta = 0$, the imaginary part does not vanish at a finite value of u. This means the quantum mechanical system is detuned similar to the classical Duffing oscillator, see Eq. (2.11).

Chapter 5

Closed and open system modes

5.1 Closed system

5.1.1 Bogoliubov transformation

In this section, we determine the spectrum of the Hamiltonian in the closed system in two ways. The Bogoliubov transformation and a symplectic diagonalization. The second method is also useful for the open dissipative system.

We define a new pair of ladder operators by $a = ub + vb^\dagger$ where u and v are complex numbers and b and $b^\dagger$ are the new ladder operators. They need to fulfill the bosonic commutation relation, $[a, a^\dagger] = 1 = [b, b^\dagger]$. We obtain the constraint $|u|^2 - |v|^2 = 1$ and is solved by hyperbolic functions with an additional complex phase, $u = e^{i\varphi_1} \cosh\theta$ and $v = e^{i\varphi_2} \sinh\theta$. Note that the transformation can be written as a matrix by

$$\begin{pmatrix} a \\ a^\dagger \end{pmatrix} = \begin{pmatrix} e^{i\varphi_1} \cosh\theta & e^{i\varphi_2} \sinh\theta \\ e^{-i\varphi_2} \sinh\theta & e^{-i\varphi_1} \cosh\theta \end{pmatrix} \begin{pmatrix} b \\ b^\dagger \end{pmatrix}. \tag{5.1}$$

By the substitution of a and $a^\dagger$ in Eq. (4.1) and looking for an angle where the off-diagonal values equal to zero the Hamiltonian can be diagonalized. The Hamiltonian in the new basis is given by

$$H = \widetilde{\omega}(\theta) b^\dagger b + [\widetilde{\varepsilon}(\theta) b^2 + \widetilde{\varepsilon}(\theta) {b^\dagger}^2] + \text{const.} \tag{5.2}$$

where $\widetilde{\varepsilon}$ needs to be zero and $\widetilde{\omega}$ represents the energy. We solve

$$\widetilde{\varepsilon} = \frac{\Delta}{2} e^{i(\varphi_1 - \varphi_2)} \cosh\theta \sinh\theta + \frac{i\varepsilon}{4} (e^{2i\varphi_1} \cosh^2\theta - e^{-2i\varphi_2} \sinh^2\theta) = 0 \tag{5.3}$$

for θ where $e^{i(\varphi_1+\varphi_2)} = i$. The solution of this equation is given by $\theta = \frac{1}{2}\tanh^{-1}(\varepsilon/\Delta)$ and the excitation spectrum results in

$$H = \tfrac{1}{2}\sqrt{\Delta^2 - \varepsilon^2}\, b^\dagger b + \text{const.}. \tag{5.4}$$

In the previous chapters, it has been shown that the system is only stable below the threshold at $|\varepsilon| = (\gamma^2 + \Delta^2)^{1/2}$. In the closed system we have $\gamma = 0$ and therefore the system is only stable for $|\varepsilon| < |\Delta|$. This can be seen in the diagonalized Hamiltonian as well, since only energies for this regime are real.

5.1.2 Symplectic diagonalization

To obtain the spectrum, the Hamiltonian can be diagonalized by a symplectic transformation. We rewrite the Hamiltonian as $H = \vec{\alpha}^\dagger H_N \vec{\alpha}$ where we define $\vec{\alpha} = (a, a^\dagger)^T$. The symplectic transformation matrix S which forms a new basis with $\vec{\beta} = S^{-1}\vec{\alpha}$, needs to conserve the bosonic commutation relation and diagonalizes the Hamiltonian at the same time. This means, S needs to fulfill

$$S^\dagger H_N S = \Omega \tag{5.5}$$

$$S^\dagger J S = J. \tag{5.6}$$

Here, Ω is a diagonal matrix which contains the spectrum and the matrix J is constructed by

$$J = [\vec{\alpha}, \vec{\alpha}^\dagger] = \begin{pmatrix} [a, a^\dagger] & [a, a] \\ [a^\dagger, a^\dagger] & [a^\dagger, a] \end{pmatrix} = \begin{pmatrix} 1 & 0 \\ 0 & -1 \end{pmatrix}. \tag{5.7}$$

To do a symplectic diagonalization H_N needs to be strictly positive [5]. This means all eigenvalues have to be positive.

In general H_N is of size $2n \times 2n$ and the non-zero entries in J change to identity matrices $\mathbb{1}$ of size $n \times n$. Here, we only have a single oscillator and therefore $n = 1$. Note that for fermions the anti-commutation relation is symmetric ($\{a, a^\dagger\} = 1$) and the diagonalization can be obtained by unitary matrices.

To find the transformation which fulfills both requirements, Eq. (5.5) and (5.6), the Hamiltonian has to be rewritten as

$$H = \frac{1}{4}\begin{pmatrix} a^\dagger & a \end{pmatrix}\begin{pmatrix} \Delta & -i\varepsilon \\ i\varepsilon & \Delta \end{pmatrix}\begin{pmatrix} a \\ a^\dagger \end{pmatrix} - \frac{\Delta}{4} \tag{5.8}$$

$$= \vec{\alpha}^\dagger H_N \vec{\alpha} + \text{const.}. \tag{5.9}$$

The next step is to solve the eigenvalue problem $H_N\vec{v} = \omega J\vec{v}$. It is useful to define an operator R [5] by

$$R\begin{pmatrix}\vec{u}\\ \vec{v}\end{pmatrix} = \begin{pmatrix}\bar{\vec{v}}\\ \bar{\vec{u}}\end{pmatrix}. \tag{5.10}$$

This operator satisfies $\{J, R\} = 0$ and $[H_N, R] = 0$, since the Hamiltonian is hermitian. Using the operator R leads to

$$RH_N\vec{v} = H_N(R\vec{v}) = \omega RJ\vec{v} = -\omega J(R\vec{v}). \tag{5.11}$$

This means, if $\vec{v}$ is an eigenvector with eigenvalue ω, then $R\vec{v}$ is an eigenvector with eigenvalue $-\omega$. Therefore, it is only necessary to find one eigenvalue and its eigenvector.

The matrix S has the normalized eigenvectors as columns. Because of Eq. (5.6), the symplectic norm is defined by $N^2 = \vec{v}^\dagger J\vec{v}$. The transformation is then given by

$$S = \frac{1}{N}\begin{pmatrix} i\varepsilon & \Delta - \omega_N \\ \Delta - \omega_N & -i\varepsilon \end{pmatrix}, \tag{5.12}$$

with $N^2 = \varepsilon^2 - (\Delta - \omega_N)^2$ and $\omega_N = (\Delta^2 - \varepsilon^2)^{1/2}$. The resulting diagonalized Hamiltonian results in

$$H = \tfrac{1}{2}\sqrt{\Delta^2 - \varepsilon^2}\, b^\dagger b + \text{const.}, \tag{5.13}$$

with $(b, b^\dagger)^T = S^{-1}(a, a^\dagger)^T$. Using Eq. (5.6) and $J^2 = \mathbb{1}$, the inverse of S is calculated by $S^{-1} = JS^\dagger J$. To check the constraint that all eigenvalues have to be positive, we solve the normal eigenvalue problem. We get that the pumping strength needs to be smaller than the absolute value of the detuning again ($|\varepsilon| < |\Delta|$). Another interesting thing to see is that for $\varepsilon = \Delta$ all eigenvalues are zero and therefore just one eigenvector exists and the diagonalization is not possible, since the symplectic transformation matrix cannot be determined. We obtain the same results and the same constraints for both methods. The solution for $\Delta > \varepsilon$ can be seen in Fig 5.1.

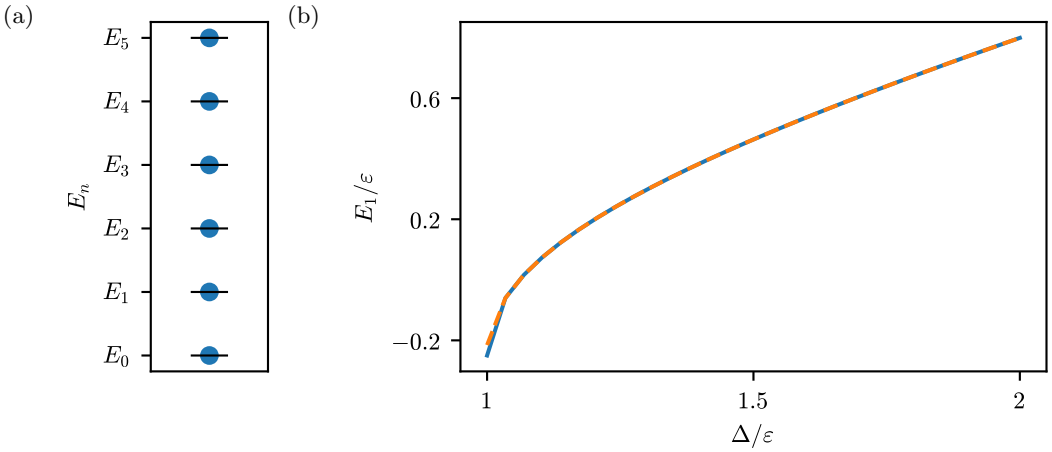

Figure 5.1: (a) Eigenspectrum of the Hamiltonian. The blue dots represent the numerically found eigenvalues while the black lines are the analytically calculated values. As expected, the eigenenergies are equidistant. (b) E_1 depending on detuning Δ. The numerical calculated values (orange dotted line) match the analytical expression (blue) very well. Just close to $\Delta = \varepsilon$ the values show a small deviance where we expect that the system is not diagonalizable.

5.2 Open system

During our calculations, we observe two recurring modes as in Eq. (2.14), (2.15) or the eigenvalues of Eq. (4.2), for resonant driving. These are

$$\lambda_- = -\frac{\varepsilon + \gamma}{2} \quad \text{and} \quad \lambda_+ = \frac{\varepsilon - \gamma}{2}. \tag{5.14}$$

In this section the Lindbladian is diagonalized by using the symplectic transformation. To do this we define new operators O_+ and O_-. The first describes the action from the left and the second one describes the action from the right, e.g. $a_+ a_-^\dagger \rho = a \rho a^\dagger$. With this definition the Lindbladian results in

$$\mathcal{L} = -i\left(H_+ - H_-\right) + \gamma\left[a_+ a_-^\dagger - \frac{1}{2}\left(a_+^\dagger a_+ + a_-^\dagger a_-\right)\right]. \tag{5.15}$$

Because the O_- operators act on the right, the commutation relation is reversed as well. We have $[a_+, a_+^\dagger] = 1 = [a_-^\dagger, a_-]$. Here, it is helpful to define new operators similar to the center of mass coordinates by

$$a_c = \frac{a_+ + a_-}{2} \qquad \text{and} \qquad a_q = a_+ - a_-, \tag{5.16}$$

with $[a_q, a_c^\dagger] = 1 = [a_c, a_q^\dagger]$. By replacing the Hamiltonian and the ladder operators in Eq. (5.15), we obtain

$$\mathcal{L} = \frac{\varepsilon}{2}\left(a_c a_q - a_c^\dagger a_q^\dagger\right) + \frac{\gamma}{2}\left(a_q a_c^\dagger - a_c a_q^\dagger - a_q^\dagger a_q\right), \tag{5.17}$$

for resonant driving. We remember from Sec. 5.1.2 that the Lindbladian needs to be rewritten into a matrix and that the commutator preserving matrix J is needed to perform the symplectic diagonalization. Since the Lindbladian is not hermitian, we can choose different right and left $\vec{\alpha}$ vectors and it is diagonalized by a right (V) and a left (W) transformation matrix. They contain the right eigenvectors $\vec{v}$ as columns and the left eigenvectors $\vec{w}$ as rows which are normalized by the symplectic norm $N^2 = \vec{w}J\vec{v}$.

The Lindbladian can be written as

$$\mathcal{L} = \frac{1}{4}\begin{pmatrix} a_q^\dagger & a_c^\dagger & a_q & a_c \end{pmatrix}\begin{pmatrix} -\gamma & -\gamma & -\varepsilon & 0 \\ 0 & \gamma & 0 & -\varepsilon \\ \varepsilon & 0 & \gamma & -\gamma \\ 0 & \varepsilon & 0 & -\gamma \end{pmatrix}\begin{pmatrix} a_c \\ a_q \\ a_c^\dagger \\ a_q^\dagger \end{pmatrix} \tag{5.18}$$

$$= \vec{\alpha_L}^\dagger L \vec{\alpha_R} = \vec{\alpha_L}^\dagger W^{-1} W L V V^{-1} \vec{\alpha_R} \tag{5.19}$$

where WLV is a diagonal matrix. The $\vec{\alpha}$ vectors fulfill

$$[\vec{\alpha_R}, \vec{\alpha_L}^\dagger] = J = \begin{pmatrix} \mathbb{1} & 0 \\ 0 & -\mathbb{1} \end{pmatrix}, \tag{5.20}$$

with identity matrices of size 2×2. In Sec. 5.1.2, we have $n = 1$ and just one mode. For the Lindbladian it is $n = 2$ and therefore two different modes are expected.

The procedure is the same as for the Hamiltonian. This means that the eigenvalue problem $L\vec{v} = \lambda J\vec{v}$ and $\vec{w}L = \vec{w}J\lambda$ is solved and the transformation matrices are built by the left and right eigenvectors. The transformation leads to two new annihilation operators, u_1 and u_2, and two new creation operators, v_1 and v_2. They fulfill $[u_i, v_j] = \delta_{ij}$ and $[u_i, u_j] = 0 = [v_i, v_j]$.

Here, the eigenvalues are $\lambda_1 = -\frac{1}{4}(\varepsilon + \gamma)$, $\lambda_2 = \frac{1}{4}(\varepsilon - \gamma)$ and $\lambda_{3,4} = -\lambda_{1,2}$. The resulting diagonal matrix is given by

$$\Lambda = WLV = \frac{1}{4}\begin{pmatrix} -(\varepsilon+\gamma) & 0 & 0 & 0 \\ 0 & \varepsilon - \gamma & 0 & 0 \\ 0 & 0 & -(\varepsilon+\gamma) & 0 \\ 0 & 0 & 0 & \varepsilon - \gamma \end{pmatrix}. \tag{5.21}$$

The Lindbladian is diagonalized and it has two different modes as expected. Therefore, it can be written as

$$\mathcal{L} = -\frac{\varepsilon+\gamma}{2} v_1 u_1 + \frac{\varepsilon-\gamma}{2} v_2 u_2 \tag{5.22}$$

where the new ladder operators are given by

$$u_1 = \frac{i}{\sqrt{2}}\left[(a_c + a_c^\dagger) + \frac{\gamma}{2(\varepsilon+\gamma)}(a_q - a_q^\dagger)\right] \tag{5.23}$$

$$u_2 = \frac{i}{\sqrt{2}}\left[-(a_c - a_c^\dagger) + \frac{\gamma}{2(\varepsilon-\gamma)}(a_q + a_q^\dagger)\right] \tag{5.24}$$

$$v_1 = \frac{i}{\sqrt{2}}(a_q - a_q^\dagger) \tag{5.25}$$

$$v_2 = \frac{i}{\sqrt{2}}(a_q + a_q^\dagger). \tag{5.26}$$

The ladder operators satisfy the commutation relation as mentioned earlier. Note that $u_i^\dagger \neq v_i$. In Eq. (5.22), it is easy to see that all eigenvalues are negative below the threshold. Therefore, the system reaches a steady state in this regime.

5.3 Single mode description

In the previous section, we have extracted two modes from the Lindbladian. We have a fast (λ_-) and a slow (λ_+) decaying mode, see Eq. (5.14). Close to the threshold λ_+ is very small and the timescale λ_+^{-1} becomes very large. The other mode has a large value and is becoming larger for bigger values of ε. Therefore, this mode is a fast decaying mode and it can be neglected in Eq. (5.22). This means that $v_1 = u_1 = 0$ which is a valid approximation when we are close to the instability threshold $\varepsilon = \gamma$. The approximated Lindbladian is given by

$$\mathcal{L} \approx \frac{\varepsilon-\gamma}{2} v_2 u_2 = i\frac{\varepsilon-\gamma}{2} x_q p_c - \frac{\gamma}{4} x_q^2 \tag{5.27}$$

where x_q and p_c fulfill the canonical commutation relation $[x_q, p_c] = i$.

To compare the dynamics of the approximated system with the full system where both modes have an impact, we calculate the steady state solutions of the occupation number operator $N = a_+ a_-^\dagger$. With this definition, the expectation value is calculated by

$$\langle N\rangle = \mathrm{Tr}(N\rho) = \mathrm{Tr}\Big(a_+ a_-^\dagger \rho\Big) = \mathrm{Tr}\Big(a\rho a^\dagger\Big) = \mathrm{Tr}\Big(a^\dagger a\rho\Big) = \langle a^\dagger a\rangle, \tag{5.28}$$

using the cyclic property of the trace. In the approximation, we have $x_c = 0 = p_q$

and so the operator is given by

$$N = \frac{1}{2}\left(p_c - \frac{i}{2}x_q\right)^2. \tag{5.29}$$

The steady state solution is shown in Fig. 5.2. The approximation fits perfectly close to the threshold and has just a small deviance for smaller values of ε. Since the system is reduced to a single mode, the computation time is significantly reduced.

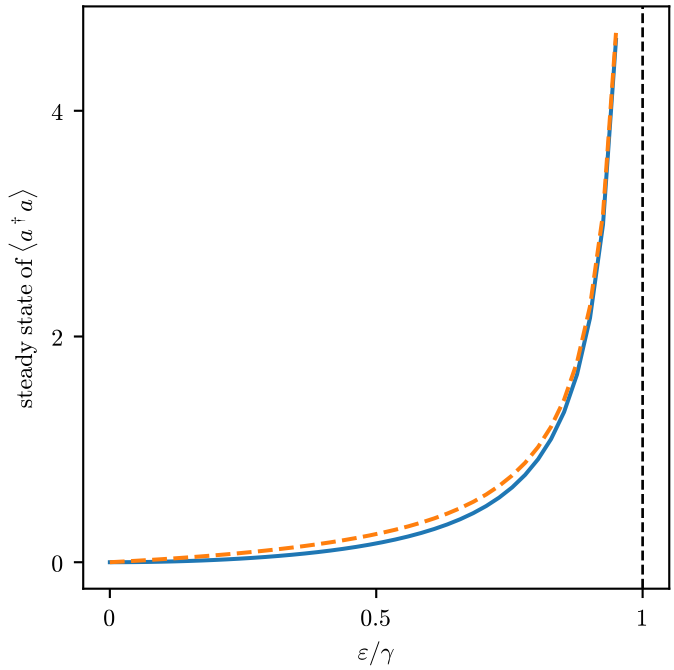

Figure 5.2: Steady state solution of $\langle a^\dagger a \rangle$ with the approximated Lindbladian (Eq. (5.27)) and approximated occupation number operator Eq. (5.29) (orange dotted line) and the exact solution (blue solid line). The approximated values fit perfectly close to the threshold (black dotted line) and show a small deviance for smaller values of ε.

Chapter 6

Conclusion and Outlook

In this thesis, the parametric instability threshold was investigated. In Ch. 2, we have discussed the classical parametric oscillator using a rotating-frame approximation and derived that the instability threshold is reached at a pumping strength of $|\varepsilon| = (\gamma^2 + \Delta^2)^{1/2}$. We have also seen that a non-linearity, as for the case of the Duffing oscillator, stabilizes the system above the threshold.

The Lindblad formalism for open quantum systems introduced in Ch. 3 is used in Ch. 4, to investigate the quantum parametric oscillator. We have demonstrated that the instability threshold matches with the classical predictions. However, the quantum oscillator reaches steady states with a non-zero expectation value of the occupation number operator already below the threshold. In contrast, the amplitude of the classical system remains zero below the threshold. This means that the quantum oscillator already has excitations below the threshold which would only be expected above the threshold from a classical view. In this chapter we have also shown that the quantum Duffing oscillator stabilizes above the threshold similar to the classical Duffing oscillator and that the threshold is washed out by quantum effects such as quantum fluctuations. The classical and the quantum dynamics even match far above the threshold with $\varepsilon \gg \gamma$ where the quantum system reaches coherent states.

In Ch. 5, we have performed the diagonalization of the Hamiltonian in two ways. The second way, the symplectic diagonalization, has been a very useful tool to diagonalize the Lindbladian as well. Here, we have extracted a slow and a fast decaying mode. By neglecting the fast decaying mode, we were able to obtain an approximation for the Lindbladian close to the threshold. It is given by

$$\boxed{\mathcal{L} = i\frac{\varepsilon - \gamma}{2} x_q p_c - \frac{\gamma}{4} x_q^2} \,. \tag{6.1}$$

Close to the threshold the steady state solutions match perfectly with the non-approximated Lindbladian. Below the threshold it shows just a small deviance to the expected results. Furthermore, we have significantly reduced the computation time of the steady state values.

In conclusion, an analytic expression for the steady state values of $\langle a^\dagger a \rangle$ is obtained. The quantum system reaches coherent states that match with the classical predictions above the threshold. Below the threshold, the steady states are characterized by the quantum parametric oscillator. We have also obtained an expression for the Lindbladian close to the threshold. How the Lindbladian of the Duffing oscillator close to the threshold can be described when quantum fluctuations are involved, is an interesting subject for further studies with perturbation theory as a possible approach.

Appendix A

Lindblad steady states

The intuitive way of determining steady state solutions is to simulate the system and wait until the system reaches a steady state. This works well when just a few steady state values are needed. For many values the computation time increases very fast. Let us consider the Lindblad Master equation again which is given by

$$\frac{\partial \rho}{\partial t} = \mathcal{L}\rho. \tag{A.1}$$

When the density matrix ρ would be a vector, the equation results in a eigenvalue problem. Since matrices form a vector space, we can transform the density matrix into a vector by [6]

$$\rho = \sum_{n,m} p_{nm} \left|n\right\rangle \left\langle m\right| \quad \rightarrow \quad \left|\rho\right\rangle = \sum_{n,m} p_{nm} \left|n\right\rangle \otimes \left|m\right\rangle . \tag{A.2}$$

When we imagine ρ as a matrix, we can think of the transformation as stacking of the transposed row vectors. To solve the Lindblad Master equation, we need to know how to vectorize a product of three matrices. This is given by

$$\left|ABC\right\rangle = (A \otimes C^T) \left|B\right\rangle . \tag{A.3}$$

To show that the expressions are the same, we calculate both sides

$$ABC = \sum A_{ij} \left|i\right\rangle \left\langle j\right| B_{kl} \left|k\right\rangle \left\langle l\right| C_{mn} \left|m\right\rangle \left\langle n\right| = \sum A_{ij} B_{jm} C_{mn} \left|i\right\rangle \left\langle n\right| \tag{A.4}$$

and

$$\begin{aligned} (A \otimes C^T) \left|B\right\rangle &= \left(\sum A_{ij} \left|i\right\rangle \left\langle j\right| \otimes C_{mn} \left|n\right\rangle \left\langle m\right|\right) \left(\sum B_{kl} \left|k\right\rangle \otimes \left|l\right\rangle\right) \\ &= \sum A_{ij} B_{jm} C_{mn} \left|i\right\rangle \otimes \left|n\right\rangle . \end{aligned} \tag{A.5}$$

When we vectorize Eq. (A.4), we get equality. With this, it is possible to rewrite the Lindbladian in Eq. (2.11). Here, we obtain

$$\widetilde{\mathcal{L}} = -i\left(H \otimes \mathbb{1} - \mathbb{1} \otimes H^T\right) + \gamma\left[a \otimes {a^\dagger}^T - \frac{1}{2}\left(a^\dagger a \otimes \mathbb{1} + \mathbb{1} \otimes (a^\dagger a)^T\right)\right] \quad \text{(A.6)}$$

for a system described by the Hamiltonian H with single photon loss and coupled to a zero-temperature environment.

The Lindblad Master equation has become a simple first order linear differential equation and is solved by $|\rho(t)\rangle = e^{\widetilde{\mathcal{L}}t}|\rho(0)\rangle$. To solve the matrix exponential, we need to know about the spectral properties of the Lindbladian.

The Lindbladian is not hermitian. This means that it has left and right eigenvectors that are not the adjoint of each other. We have

$$\widetilde{\mathcal{L}}|v_n\rangle = \lambda_n|v_n\rangle \quad \text{(A.7)}$$

$$\langle w_n|\widetilde{\mathcal{L}} = \langle w_n|\mu_n. \quad \text{(A.8)}$$

By multiplying $\langle w_n|$ to the first equation and $|v_n\rangle$ to the second and subtracting them, we get

$$(\lambda_n - \mu_n)\langle w_n|v_n\rangle = 0. \quad \text{(A.9)}$$

The left and right eigenvectors have the same eigenvalues and they build an orthonormal basis. Therefore, the Lindbladian is diagonalized by $\Lambda = V\widetilde{\mathcal{L}}W$ where Λ is the diagonal matrix containing the eigenvalues and W and V transformation matrices that contain the left and right eigenvectors as rows and columns. Then, the matrix exponential is solved by

$$e^{\widetilde{\mathcal{L}}t} = Ve^{\Lambda t}W = \sum_n e^{\lambda_n t}|v_n\rangle\langle w_n|. \quad \text{(A.10)}$$

To describe the physical dynamics, we need more information about the eigenvalues and eigenvectors of the Lindbladian.

An important property of the density matrix is that it is normalized by $\mathrm{Tr}(\rho) = 1$. Here we have, $\mathrm{Tr}(A^\dagger B) = \sum \bar{a_{ji}} b_{ji} = \langle A|B\rangle$. This means, we can write the normalization as $\mathrm{Tr}(\rho) = \langle\mathbb{1}|\rho\rangle$ where $\langle\mathbb{1}|$ is the vectorized identity matrix. The identity matrix has another property. When multiplying $\langle\mathbb{1}|$ to the vectorized Lindblad Master equation, we obtain

$$0 = \langle\mathbb{1}|\frac{\partial}{\partial t}|\rho\rangle = \langle\mathbb{1}|\widetilde{\mathcal{L}}|\rho\rangle. \quad \text{(A.11)}$$

This has to be true for any arbitrary density matrix. This means, the vectorized identity matrix is always the left eigenvector of any Lindbladian with

eigenvalue 0. When there is a left eigenvector, there also has to be a right eigenvector. It corresponds to the steady state solution, $|\rho_{ss}\rangle$. The general solution can be written as

$$|\rho(t)\rangle = |\rho_{ss}\rangle \langle \mathbb{1}|\rho(0)\rangle + \sum_{n,\lambda_n \neq 0} e^{\lambda_n t} |v_n\rangle \langle w_n|\rho(0)\rangle \tag{A.12}$$

where $\langle w_n|\rho(0)\rangle$ are coefficients, related to the initial condition and $\langle \mathbb{1}|\rho(0)\rangle$ equals one, due to normalization. This means as long as all eigenvalues have a negative real part, the system reaches the steady state for large times. The real part of the eigenvalues tells us about the relaxation time of the different terms in Eq. (A.12) and therefore give us the relevant time scale. With this knowledge, we can calculate the expectation value in the steady state of any time-independent observable O by

$$\langle O \rangle = \frac{\mathrm{Tr}(O\rho_{ss})}{\mathrm{Tr}(\rho_{ss})} = \frac{\langle O|\rho_{ss}\rangle}{\langle \mathbb{1}|\rho_{ss}\rangle} = \frac{\langle \mathbb{1}| O |\rho_{ss}\rangle}{\langle \mathbb{1}|\rho_{ss}\rangle}. \tag{A.13}$$

Here, we divide by the trace, since numerical calculations do not give us the right normalization of the eigenvectors.

Appendix B

Numerical Methods

B.1 Forward Euler method

To check our analytical calculations, we can use numerical evolutions of the system and compare the results. When differential equations cannot be solved analytically anymore, we can also use the numerical evolution to obtain a prediction of the dynamics of the system. To do this, we use the forward-Euler method. It works for first-order differential equations, $y'(t) = f(t, y(t))$, which is the case in this thesis for the Lindblad Master equation. Then, the solution can be constructed by

$$y_{n+1} = y_n + hf(t_n, y_n) \tag{B.1}$$

where h is the step size between two values. For large values of h the solution might not be accurate and can even give false results. To get a good estimation of the solution, small values for h are recommended.

B.2 Matrix representation of operators

To evolve the Lindblad Master equation numerically, we need the matrix representation of the operators. These matrices can be determined by the effect on the states which span the Hilbert space. In general, the space is infinitely large. To use numerical evolutions, we cannot use infinitely large matrices, since computers have a limited amount of memory. This means, we have to limit the space. The evolutions in this thesis uses two bases, the Fock basis and the position basis.

We start with the Fock basis. Here, we define a highest state N to limit the space. The effect of the ladder operators a and $a^\dagger$ on a Fock state $|n\rangle$ are $a|n\rangle = \sqrt{n}\,|n-1\rangle$ and $a^\dagger|n\rangle = \sqrt{n+1}\,|n+1\rangle$. This way, the matrices are

given by

$$a = \begin{pmatrix} 0 & \sqrt{1} & 0 & & & \\ & \ddots & \sqrt{2} & \ddots & & \\ & & & \sqrt{3} & & \\ & & & & \ddots & 0 \\ & & & & & \sqrt{N} \\ & & & & & 0 \end{pmatrix} \tag{B.2}$$

$$a^\dagger = \begin{pmatrix} 0 & & & & & \\ \sqrt{1} & \ddots & & & & \\ 0 & \sqrt{2} & & & & \\ & \ddots & \sqrt{3} & & & \\ & & & \ddots & & \\ & & & 0 & \sqrt{N} & 0 \end{pmatrix} \tag{B.3}$$

where $|n\rangle$ is

$$|n\rangle = \begin{pmatrix} 0 \\ \vdots \\ 1 \\ 0 \\ \vdots \\ 0 \end{pmatrix}, \tag{B.4}$$

with the 1 at the n-th position. Choosing high values of N ensures that the evolution is accurate, because at no point of the evolution we leave the Hilbert space by multiple applications of the Lindbladian.

The second basis we use is the position basis where we use the definition of the ladder operators, $a = \frac{1}{\sqrt{2}}(x + ip)$. Here, x is the normalized position operator, with $x\,|x\rangle = x\,|x\rangle$, and P the normalized impulse, $p\,|x\rangle = -i\frac{d}{dx}\,|x\rangle$. For the parabolic potential of the harmonic oscillator, the probability distribution outside of the potential gets exponentially small. For higher states the potential and therefore the distribution gets wider. This means, we have to choose a sufficiently large interval for x and a small division l of this range. The needed

matrices given by

$$x = \begin{pmatrix} -x & 0 & & & \\ 0 & -x+l & \ddots & & \\ & \ddots & \ddots & & \\ & & & x-l & 0 \\ & & & 0 & x \end{pmatrix} \tag{B.5}$$

$$\frac{d}{dx} = \frac{1}{2l} \begin{pmatrix} 0 & 1 & & & \\ -1 & 0 & 1 & & \\ & -1 & \ddots & \ddots & \\ & & \ddots & \ddots & 1 \\ & & & -1 & 0 \end{pmatrix} \tag{B.6}$$

where $|x\rangle$ has the 1 at the m-th place when the position is given by $-x + m \cdot l$. The difference quotient is mostly chosen as $(f(x+l) - f(x))/l$. Here, we choose a different form to keep the impulse operator hermitian, $(f(x+l) - f(x-l))/2l$. Because of the sparse form of the matrices, they are easy to implement. In the Fock basis, we only have one parameter to adjust, the highest state. In the position basis, we have two parameters that result in big matrices to get accurate results. This means it is in general faster and more accurate to operate in the Fock basis.

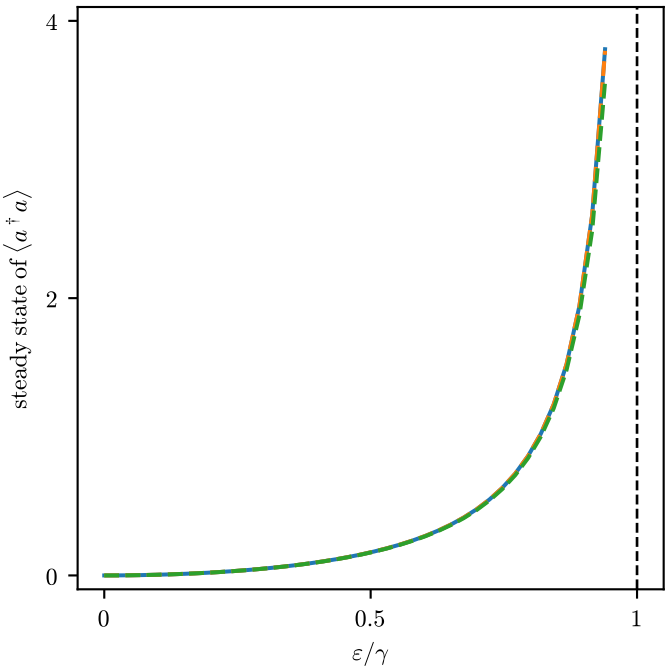

Figure B.1: Steady state solutions for $\langle a^\dagger a \rangle$. Analytical (blue), Fock basis (orange) and position basis (green). The solution in the Fock basis fits perfectly, while the position basis shows a small deviance close to the threshold. In addition, the calculation in the position basis takes a lot more time than in the Fock basis.

Acknowledgements

I want to thank my supervisor Fabian Hassler for making this thesis possible, introducing me into this interesting branch of physics and being a great teacher. I would also like to give special thanks to Lisa Arndt for every Zoom call, for always taking time for answering my questions and for the best mentoring I could have asked for. Thanks to both of you for the close supervision.

Bibliography

[1] A. Das and S.K. Das. *Microwave Engineering*. Tata McGraw-Hill Publishing Company Limited (2000).

[2] J.B. Calvert. *Varactors*. `http://mysite.du.edu/~etuttle/electron/elect40.htm`.

[3] G. Lindblad. *On the Generators of Quantum Dynamical Semigroups*. Springer, Communications in Mathematical Physics (1976).

[4] M. Czakon. *QM (Quantum mechanics script)*. (2020).

[5] J.L. Van Hemmen. *A note on the diagonalization of quadratic boson and fermion hamiltonians*. Springer, Zeitschrift für Physik B Condensed Matter (1980).

[6] D.R. Gilchrist A., Terno and C.J. Wood. *Vectorization of quantum operations and its use*. arXiv:0911.2539 (2009).